Unraveling intra-aggregate structural disorder using single-molecule spectroscopy

Kunsel, T.; Loehner, A.; Mayo, J. J.; Koehler, J.; Jansen, T. L. C.; Knoester, J.

Published in:
Journal of Chemical Physics

DOI:
10.1063/5.0023551

Publication date:
2020

The Journal of Chemical Physics

Unraveling intra-aggregate structural disorder using single-molecule spectroscopy

Cite as: J. Chem. Phys. **153**, 134304 (2020); https://doi.org/10.1063/5.0023551
Submitted: 30 July 2020 . Accepted: 14 September 2020 . Published Online: 05 October 2020

T. Kunsel, A. Löhner, J. J. Mayo, J. Köhler, T. L. C. Jansen, and J. Knoester

COLLECTIONS

Paper published as part of the special topic on Excitons: Energetics and Spatio-temporal Dynamics

This paper was selected as an Editor's Pick

The Journal of Chemical Physics ARTICLE scitation.org/journal/jcp

Unraveling intra-aggregate structural disorder using single-molecule spectroscopy

Cite as: J. Chem. Phys. 153, 134304 (2020); doi: 10.1063/5.0023551
Submitted: 30 July 2020 • Accepted: 14 September 2020 •
Published Online: 5 October 2020

T. Kunsel,[1] A. Löhner,[2] J. J. Mayo,[1] J. Köhler,[2,3,4] T. L. C. Jansen,[1] and J. Knoester[1,a)]

AFFILIATIONS

[1]University of Groningen, Zernike Institute for Advanced Materials, Nijenborgh 4, 9747 AG Groningen, The Netherlands
[2]Spectroscopy of Soft Matter, University of Bayreuth, Universitätsstraße 30, 94557 Bayreuth, Germany
[3]Bavarian Polymer Institute, University of Bayreuth, Universitätsstraße 30, 94557 Bayreuth, Germany
[4]Bayreuth Institute of Macromolecular Research (BIMF), University of Bayreuth, Universitätsstraße 30, 94557 Bayreuth, Germany

Note: This paper is part of the JCP Special Topic on Excitons: Energetics and Spatio-Temporal Dynamics.
[a)]**Author to whom correspondence should be addressed:** j.knoester@rug.nl

ABSTRACT

Structural disorder within self-assembled molecular aggregates may have strong effects on their optical functionality. Such disorder, however, is hard to explore using standard ensemble measurements. In this paper, we report on the characterization of intra-aggregate structural disorder through a linewidth analysis of fluorescence excitation experiments on individual zinc-chlorin (ZnChl) nanotubular molecular aggregates. Recent experiments suggest an anomaly in the linewidths of the two absorption bands that dominate the spectra: the higher-energy bands on average show a smaller linewidth than the lower-energy bands. This anomaly is explored in this paper by analyzing and modeling the correlation of the two linewidths for each aggregate. We exploit a Frenkel exciton model to show that the experimentally observed correlation of linewidths and other statistical properties of the single-aggregate spectra can be explained from small variations of the molecular orientations within individual aggregates.

I. INTRODUCTION

Low-dimensional supramolecular aggregates bridge the gap between single molecules and bulk phases and reveal properties that make them suitable for nanoscale functional materials. Important examples are aggregates formed by dye molecules, which show interesting optical properties, including sharp absorption lines,[1–3] ultrafast emission,[4,5] enhanced and anomalous nonlinear optical response,[6–8] and fast and long-range excitation energy transport.[9,10] Nature also exploits supramolecular aggregates for specific functions. Well-known biological functions are light harvesting and transport of electronic excitation energy, performed by photosynthetic antenna systems, which are aggregates of tens to many thousands of biological dye molecules that occur in higher plants, certain bacteria, and algae.[11–19]

The opto-electronic properties of supramolecular aggregates are highly sensitive to the details of the packing of the molecules because excitation transfer interactions and charge-transfer integrals, which dictate these properties and the underlying collective excited states (excitons), depend sensitively on distances between molecules and their mutual orientations.[20–23] Consequently, structural disorder in dye aggregates may strongly influence their optical properties and excited state dynamics, such as exciton diffusion. Static disorder in the excitation energies of individual molecules within aggregates (diagonal disorder), imposed by variations in the local environment that are slow compared to the experimentally relevant time scale, has been considered in many studies, both phenomenologically[24–29]—by comparing spectra of model aggregates with disorder to the experiment—and by using more sophisticated methods.[30–34] This type of disorder leads to localization of the exciton states and affects optical properties such as the optical linewidths, optical nonlinearities, and excitation energy transport.[7,24,25,35–40] Structural disorder, primarily resulting in variations in the intermolecular interactions, which also ultimately leads to line

broadening and altered transport properties, has been studied less frequently.[25,41]

For functionality, it is of interest to distinguish variation between aggregates (inter-aggregate disorder) and fluctuations within aggregates (intra-aggregate disorder).[42] For example, in the case of transport properties, static disorder within aggregates is more detrimental than static differences between aggregates. In the extreme case where each individual aggregate is completely homogeneous and only inter-aggregate disorder exists (i.e., certain parameters differ systematically between aggregates), the transport properties within each aggregate will not be hampered by the disorder. In the opposite case where static disorder occurs within aggregates, while on average the aggregates are all the same, the transport properties may be strongly affected by the disorder. Thus, it is important to disentangle what disorder should be attributed to single aggregates (on the time scale relevant to the experiment considered) and what disorder derives from differences between aggregates. For this purpose, the (optical) characterization of individual aggregates is essential.

Fluorescence excitation experiments on individual dye aggregates have been carried out since 1999, both for biological light harvesting complexes[12,43] and for synthetic aggregates.[44] Experiments have revealed strong variations between individual aggregates, even for very large aggregates consisting of many thousands of molecules, where one would expect that optical properties average out over the many internal degrees of freedom.[44] Recent experiments on single semi-synthetic zinc-chlorin (ZnChl) aggregates are of particular interest.[45] These aggregates have a tubular shape with a diameter of a few nm and a length of the order of 100 nm up to several micrometers.[46] Synthetic tubular molecular aggregates have attracted much attention recently[47–59] because they bear an interesting morphological resemblance to the bacteriochlorophyll aggregates that occur in chlorosomes—the highly efficient light harvesting antennae of green sulfur bacteria.[43,60–64] In contrast to these natural systems, which consist of mixtures of several types of bacteriochlorophyll molecules and therefore suffer from an inherent large degree of heterogeneity, semi-synthetic ZnChl nanotubes are prepared from chemically identical molecules. Despite this, recent fluorescence excitation experiments on individual ZnChl nanotubes show strong variations between each other. These variations have been explained in terms of relatively small differences in the structure between different aggregates, in particular, from differences of a few degrees in the orientation of the molecules within the aggregate and the helical angle of its structure.[45] In the analysis reported in Ref. 45, based on a Frenkel exciton model, these angles were kept constant within each aggregate and only varied *between* aggregates (inter-aggregate structural disorder). While this analysis yielded good fits of theory to the experiment, it also left questions unanswered: in particular related to the nature and relative magnitude of the linewidths of the two absorption peaks that occur in these nanotubes. The higher-energy bands on average showed smaller widths than the lower-energy ones, suggesting intra-aggregate inhomogeneity.

In this paper, we report on a detailed analysis of the linewidth correlation within individual ZnChl aggregates and show that the anomaly can be understood from intra-aggregate disorder, namely, from variation of the molecular orientations *within* individual aggregates. We consider two situations, namely, a segment-like variation of the orientations and a more continuous variation. We show that, in particular, the latter model offers a broad understanding of the statistical properties of the single-aggregate spectra, not only of the linewidth anomaly but also of the distribution of peak positions.

The remainder of this paper is organized as follows. In Sec. II, we briefly describe the general features of the spectra for single ZnChl nanotubular aggregates, and we present the measured correlation of the widths of both absorption lines within individual aggregates. Next, in Sec. III, we introduce the Frenkel exciton model used to interpret the experimental data, and we analyze whether or not disorder in each one of the three angles defining the molecular packing can potentially explain the anomaly; moreover, we rule out alternative explanations, such as intra-aggregate diagonal disorder. In Sec. IV, we present and discuss our results from spectral simulations for the segment and continuous disorder models and compare to the experiment. Finally, in Sec. V, we conclude.

II. EXPERIMENTAL CORRELATION OF LINEWIDTHS

In Ref. 45, polarization dependent fluorescence excitation spectra of individual ZnChl nanotubes were reported. It was found that the spectral properties of individual tubular aggregates varied significantly. A more quantitative analysis revealed that for all nanotubes considered, the spectrum could be interpreted in terms of two dominant optical transitions with mutually perpendicular transition dipoles. This is consistent with having highly delocalized exciton states in tubular aggregates,[37,38] which have optical selection rules such that there is one super-radiant exciton transition with its transition dipole along the tube's axis and two degenerate ones (usually higher in energy than the first transition) with their transition dipoles perpendicular to the axis.[65] The experiments were further analyzed in terms of a Frenkel exciton model, which revealed that small variations in the molecular orientations between different aggregates could explain the differences in their respective polarization resolved spectra. In this exciton model, the orientation angles were kept identical for all molecules within each tube so that only inter-aggregate disorder was allowed for. This fitting procedure yielded good fits, where the angles had to be varied within small intervals of only a few degrees; the linewidths of the two exciton transitions were used as fit parameters.

Both the two-state fitting procedure and the fits based on a microscopic Frenkel exciton model generally seemed to lead to a smaller linewidth for the higher-energy state than for the lower-energy one, which would be counter-intuitive if one assumes that these widths are homogeneous and lifetime dominated. For lifetime dominated widths, one expects that intraband relaxation leads to larger values for the upper-energy states than the lower-energy ones. We therefore refer to the observation as the linewidth anomaly. The histograms reported in the supplementary information of Ref. 45 suggest that, indeed, this anomaly exists since the distribution of widths found for the lower-energy exciton states is shifted upward compared to the one for the higher-energy state. A clear proof that, indeed, the anomaly is characteristic for nearly all tubes is shown in the correlation plot of Fig. 1. In Fig. 1, each data point represents the linewidths (full width at half maximum—FWHM) obtained from the two-state fit for one individual aggregate, with

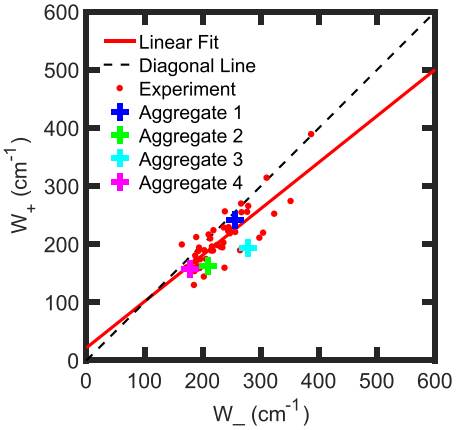

FIG. 1. Correlation between the linewidths of the upper and lower-exciton transitions obtained from the two-state fits of the polarization dependent fluorescence excitation spectra on 52 individual nanotubular ZnChl aggregates, as performed in the study reported in Ref. 45. Each red dot in the graph specifies the full width at half maximum (FWHM) for the lower (W_-) and higher (W_+) exciton states. The crosses represent the experimental data for the four specific nanotubes analyzed in Ref. 45. The black dashed line is the diagonal of the graph, while the red solid line represents the best linear regression of all data points, with a slope of 0.8 and an offset of 21.7 cm^{-1}.

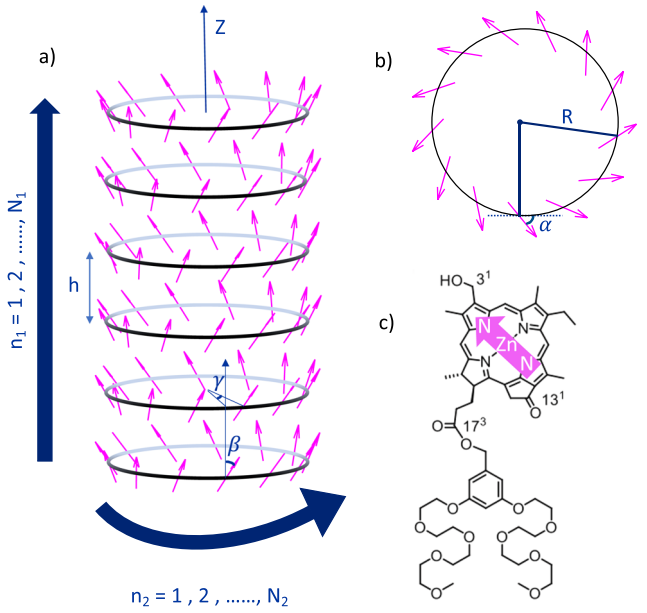

FIG. 2. (a) Structure of the tubular aggregate, consisting of a perpendicular stack of N_1 rings of radius R, each with N_2 ZnChl molecules, presented by their transition dipoles that are shown as magenta arrows. The distance h between adjacent rings and the helical angle γ over which adjacent rings are rotated relatively to each other are indicated, as is the angle β between the molecular transition dipole and the tube's axis. (b) Top view of a single ring, indicating the angle α that further specifies the orientation of the molecular dipole (see text). (c) Structure of the ZnChl monomer with its transition dipole vector represented by the magenta arrow.

the width of the lower state, W_-, specified along the horizontal axis of the graph and the width of the upper state, W_+, along the vertical axis. A vast majority of the data points, representing the analysis of the experiments on 52 individual tubes, lie below the diagonal of this graph, clearly establishing the general existence of the anomaly. This implies that homogeneous (lifetime) broadening alone cannot explain the exciton linewidth, leaving us with some source of intra-aggregate disorder. In addition, Fig. 1 also reveals a positive correlation between both linewidths, indicated by the red line, which is a least-square regression. The analysis in the remainder of this paper aims at identifying the source of disorder and quantifying its magnitude.

III. EXCITON MODEL AND SOURCE OF DISORDER

A. Model

The model structure we use for the nanotubular aggregates of ZnChl molecules (monomers) is depicted schematically in Fig. 2. It consists of a perpendicular stack of N_1 equidistant rings, on each one of which N_2 equidistant molecules are placed. Each molecule is identified by a position vector $\mathbf{n} = (n_1, n_2)$, where n_1 is the ring on which it resides and n_2 gives the position in the ring. For modeling the optical properties of the nanotube, the relevant molecular optical transition is the Q_y transition, with a transition dipole of magnitude 4.5 D pointing diagonally within the porphyrin ring where the optical transition takes place. This transition dipole and the interactions between the dipoles of different molecules govern the collective excited states and optical properties of the nanotube. For this reason, it suffices to represent each molecule by its transition dipole. Hence, for the purpose of modeling its optical properties, the nanotube is characterized by its radius R and the number of molecules per ring, N_2, by the distance h between two adjacent rings, by the helical angle γ that describes the relative rotation angle between two adjacent rings, and by the orientations of the molecular transition dipoles in the tube. The latter are described by the angle β between the dipole and the tube's axis and the angle α between the projection of the dipole on the plane of the ring relative to the local tangent to the ring (for perfect tubular symmetry, α is the same for all molecules and so is β). All these quantities are indicated in Fig. 2. The tube's length $L = N_1 h$ is assumed long enough not to affect its absorption spectrum anymore. This stack of ring representation may be derived from rolling a two-dimensional lattice of molecules on a cylinder of radius R.[28]

The collective linear optical properties of the aggregate are described by the Frenkel exciton Hamiltonian,

$$H = \sum_{\mathbf{n},\mathbf{m}} H_{\mathbf{nm}} |\mathbf{n}\rangle\langle\mathbf{m}| = \sum_{\mathbf{n}} \hbar\omega_{\mathbf{n}} |\mathbf{n}\rangle\langle\mathbf{n}| + \sum_{\mathbf{n},\mathbf{m}}{}^{*} V_{\mathbf{nm}} |\mathbf{n}\rangle\langle\mathbf{m}|, \qquad (1)$$

where $|\mathbf{n}\rangle$ is the state with molecule $\mathbf{n}$ in its Q_y excited state and all other molecules in their ground states, $\hbar\omega_{\mathbf{n}}$, represent the excitation energy of molecule $\mathbf{n}$, $V_{\mathbf{nm}}$ is the excitation transfer interaction between the transition dipoles of molecules $\mathbf{n}$ and $\mathbf{m}$, and the asterisk on the summation excludes terms with $\mathbf{n} = \mathbf{m}$. The above Hamiltonian allows for disorder in the transition energies and interactions; possible sources of disorder will be considered below.

The qth eigenvalue (E_q) and eigenvector ($a_{q\mathbf{n}}$) of the matrix $H_{\mathbf{nm}}$ give the energies and site amplitudes, respectively, of the qth

exciton state. Assuming that the emission quantum yield does not depend on the emission wavelength, the fluorescence excitation spectrum measured in single-aggregate spectroscopy is identical to the aggregate's absorption spectrum, which reads[25]

$$I(E) = \sum_q |\vec{\mu}_q \cdot \vec{e}|^2 \frac{\Gamma_q}{(E - E_q)^2 + \Gamma_q^2}, \tag{2}$$

where E denotes the photon energy and $\vec{e}$ is the polarization direction of the light. Furthermore, $\vec{\mu}_q = \sum_{\mathbf{n}} a_{q\mathbf{n}} \vec{\mu}_{\mathbf{n}}$ denotes the transition dipole of the qth exciton state ($\vec{\mu}_{\mathbf{n}}$ is the transition dipole of molecule $\mathbf{n}$), and Γ_q is its homogeneous linewidth. Note that in this study, we are interested in the spectra of individual aggregates, and hence, in contrast to most other theoretical studies of molecular aggregates, we do not perform an average over disorder realizations.

Before turning to the study of disorder, it is useful to describe the generic shape of the spectrum for the above model. For long tubes, the absorption spectrum shows two bands, one polarized parallel to the axis of the cylinder, deriving from a super-radiant state with oscillator strength $N_1 N_2 \cos^2 \beta$ (in units of that of a monomer) and one polarized perpendicular to it, deriving from two degenerate transitions, both with oscillator strength $\frac{1}{2} N_1 N_2 \sin^2 \beta$.[65] Both bands are redshifted relative to the monomer transition energy (J-bands) and positioned close to the lower-exciton band edge, where (usually) the lowest-energy band is the one polarized parallel to the tube's axis and the higher-energy one is polarized perpendicular to the axis. In the polarization resolved experiments analyzed here, the tubes are lying with their axes parallel to the substrate, and only one of the perpendicular transitions is observed, implying that the ratio of oscillator strengths observed in the perpendicular and parallel direction equals $\frac{1}{2} \tan^2 \beta$. For ZnChl nanotubes, this ratio is of the order of unity[45] implying an angle β of about 55° (also see Sec. III B).

B. Sources of intra-aggregate disorder

As argued in Sec. II, single-aggregate experiments suggest that a certain degree of disorder exists within individual aggregates, in order to explain that the lower-exciton states generally have a larger linewidth than the upper ones. The above model allows for a variety of sources of disorder, for instance, in the molecular transition energies, deriving from random matrix or solvent shifts, and in the interactions, deriving from structural disorder. In this subsection, we investigate what type of disorder, in principle, may explain the linewidth anomaly.

We first consider the possibility of disorder in the molecular transition energies $\hbar\omega_{\mathbf{n}}$. This is the most commonly considered type of disorder, responsible for exciton localization, a rather weak effect in tubular aggregates.[37,38] In ensemble spectra, such disorder leads to line broadening, which to some extent is mitigated by exchange narrowing.[3,25] While probably this type of disorder also plays a role in ZnChl nanotubes, it does not lead to a natural explanation of the linewidth anomaly. The reason is that the upper-energy J band derives from two degenerate transitions, which upon adding disorder would mix and repel each other, leading to stronger line broadening than occurs for the lower-energy J band.[66] This is the opposite effect of the observed anomaly. For this reason, we do not consider this type of disorder as dominant in the line broadening and will ignore it.

Next, we consider shape variations of the tube. Based on previous results, we exclude variation of R and N_2. Electron microscopy and atomic force microscopy images of ZnChl nanotubes reveal that their diameter is very uniform along the tubes,[46] giving a well-defined radius of $R = 1.68$ nm, and energy minimization of model ZnChl tubes showed that given the radius, N_2 is well-determined at $N_2 = 13$.[45] We note in passing that, even if variations in N_2 would occur, this would not explain the anomaly because in a tubular aggregate, the position of the transition polarized parallel to its axis generally is much less sensitive to N_2 than the position of the ones polarized perpendicular to it,[28,55] implying that disorder in N_2 would lead to more broadening of the upper band than the lower band. Another obvious shape variation for tubes is an elliptical deformation. Such deformation would mainly lead to mixing of the two degenerate states contributing to the upper J band,[67,68] thereby again leading to a stronger broadening for the upper J band than the lower J band, so that it does not explain the anomaly.

Along with fixing N_2 (R), the energy minimization calculations in Ref. 45, also set a well-determined value for the inter-ring distance h, namely, $h = 0.67$ nm. However, these calculations did leave a relatively large freedom in the angles α and β that describe the molecular orientations and in the helical angle γ, a freedom that was used in Ref. 45 to explain the differences in the polarization resolved spectra between individual tubes, by choosing slightly different sets of angles for each aggregate; within each aggregate, the angles were chosen constant so that in Ref. 45, only inter-aggregate disorder was considered. By contrast, here, we will explore the possibility of variation of any of these three angles *within* individual tubes to explain the linewidth anomaly as well as other statistical properties of the spectra of single ZnChl nanotubes. This intra-aggregate orientational disorder will lead to disorder in the interactions $V_{\mathbf{nm}}$. One may also argue that interaction disorder will result in a larger broadening of the higher-energy J band as it also lifts the degeneracy of the two contributing states. However, there is an additional immediate effect on the position of the exciton states because their energies linearly depend on the interactions (e.g., the energy of the totally symmetric exciton state in an ordered aggregate is shifted away from the monomer transition energy by an amount given by the sum of all interactions between one molecule and all the other ones).

In order to assess whether disorder in any one of the parameters α, β, or γ may, in principle, explain the linewidth anomaly, we calculated the dependence of the positions $E_\parallel$ and $E_\perp$ of the super-radiant exciton states polarized parallel and perpendicular, respectively, to the tube's axis for homogeneous aggregates (no disorder) on each one of these parameters individually, while keeping the other two fixed. In this analysis, we used $R = 1.68$ nm, $N_2 = 13$, and $h = 0.67$ nm for the tube's radius, the number of molecules per ring, and the inter-ring distance, respectively, which, as explained above, apply for the ZnChl nanotubes; for the length of the tube, we used $N_1 = 1000$ rings, which makes the physical length ($N_1 h$) fall inside the typical experimental range[46] and ensures that the absorption spectrum has reached the long-tube limit. Figure 3 displays the results for aggregates where the base choice for the parameters is taken identical to their values used to fit the spectra for aggregate 1 studied in Ref. 45, i.e., $\alpha_1 = 39.9°$, $\beta_1 = 54.2°$, and $\gamma_1 = 10.0°$. Thus, in order to study the α dependence of the two exciton positions, β and γ are kept fixed

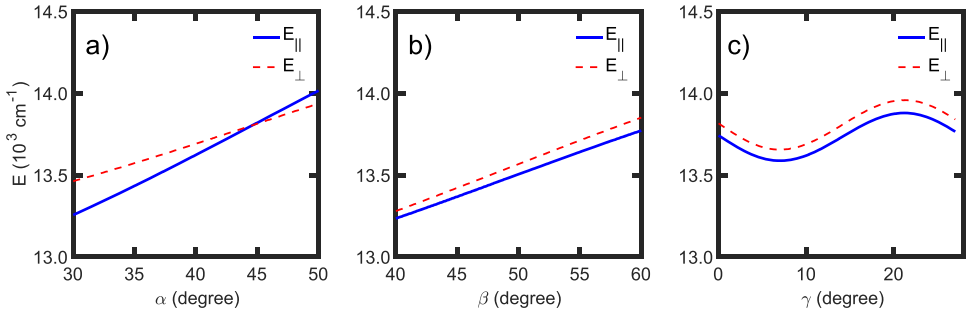

FIG. 3. Energies of the super-radiant exciton transitions polarized parallel ($E_\parallel$, blue solid line) and perpendicular ($E_\perp$, red dashed line), respectively, to the tube's axis, calculated for long homogeneous aggregates (N_1 = 1000) as a function of the angles α (a), β (b), and γ (c) (see text for details). The other structural parameters were fixed at R = 1.68 nm, h = 0.67 nm, and N_2 = 13. The transition energy and dipole of a single molecule were taken to be $\hbar\omega_0$ = 13 939 cm^{-1} and 4.5 D, respectively.[45]

at the values β_1 and γ_1, respectively, while α is varied over a certain range around α_1 [Fig. 3(a)]. Similarly, the dependencies on the other two angles are obtained. We found that the effects observed in Fig. 3 are generic and are also obtained for other base choices of the three angles, valid for the three other aggregates that were studied in detail in Ref. 45.

It is clear from Fig. 3 that the dependencies of the optically dominant exciton transitions on both β and γ are roughly equally strong, implying that intra-aggregate disorder in these angles would not lead to more line broadening for the lower-energy transition than for the higher-energy one. By contrast, Fig. 3(a) clearly shows that the parallel transitions (which for most parameter values are the lower-energy one) are more sensitive to α than the perpendicular one. As a result, intra-aggregate disorder in α would typically lead to larger broadening for the lower-energy transition and, thus, may explain the linewidth anomaly. In Sec. IV, we will present numerical results for the spectra of individual tubular aggregates accounting for intra-aggregate disorder in the molecular orientations and explore to what extent this may explain the magnitude of the anomaly as well as other statistical properties of the spectra.

IV. RESULTS

We simulated single-aggregate absorption spectra for two models of disorder in the angle α. In all calculations, we used the following fixed structural parameters, appropriate for ZnChl nanotubes:[45] R = 1.68 nm for the tube's radius, N_2 = 13 for the number of molecules per ring, and h = 0.67 nm for the inter-ring distance (see also Sec. III B); furthermore, we set all molecular transition energies equal to $\hbar\omega_{\mathbf{n}} = \hbar\omega_0$ = 13 939 cm^{-1}. The transfer interactions $V_{\mathbf{nm}}$ were calculated from the electrostatic interaction between the transition dipoles of the two molecules considered, with magnitudes 4.5 D and directions imposed by the molecular positions in the tube and the orientations as given by α and β. The angles α, β, and γ, or their disorder distributions, will be specified below. The tube's length N_1 considered depends on the disorder model, as will be explained below. Finally, the homogeneous linewidth for all exciton transitions was (unless indicated otherwise) taken to be Γ_q = 50 cm^{-1}; no experimental information is available for this parameter.

A. Two models of disorder

Two different ways were considered to account for the disorder in the molecular orientations. In the first model, each aggregate is considered as a collection of non-interacting segments of different lengths that only differ in the particular value for α that applies to the entire segment; the values for the angles β and γ are taken equal for all segments within one aggregate, i.e., no intra-aggregate disorder was included in these angles. Each segment is assumed long enough so that their exciton transition energies have saturated, i.e., have tended toward the infinite-tube values. Segment (or domain) models of disorder have been used in various studies.[69–71] Here, the strength of this model lies in its simplicity and the fact that it allows for direct simulation of the experimental spectra of individual aggregates with relative ease. In the segment model, the disorder realization of each individual aggregate is characterized by a histogram that indicates for each α interval the fraction of rings in the aggregate in which the molecules have an orientation characterized by an α value that falls within this interval (in other words, the histogram counts the added lengths of all segments that have an α value within this interval). For a particular aggregate whose experimental polarization resolved fluorescence excitation spectrum was measured, the specific realization of the disorder histogram that characterizes the aggregate can be obtained by adjusting the heights of the histogram in each α bin such that the calculated spectrum agrees with the experiment. This procedure is explained in more detail in Sec. IV B and used to fit the spectra of the four particular aggregates also studied in more detail in Ref. 45.

In the second disorder model, we allow for a continuous variation of α along the tube. Particularly, we will assume that α is constant within each ring but varies along the tube with a specific correlation length, by taking the α values for all rings from the correlated multivariate Gaussian distribution,

$$P(\alpha_1,\ldots,\alpha_{N_1}) = ((2\pi)^{N_1}\det(C))^{-1/2}\exp\Bigg[-\frac{1}{2}\sum_{n,m=1}^{N_1}(C^{-1})_{nm} \times (\alpha_n - \langle\alpha\rangle)(\alpha_m - \langle\alpha\rangle)\Bigg]. \quad (3)$$

Here, α_n denotes the angle α in the nth ring, $\langle\alpha\rangle$ is the mean α value, which is equal for all rings and all aggregates, and C is the covariance

matrix with matrix elements,

$$C_{nm} = \sigma_\alpha^2 \exp(-|n-m|/L_c), \tag{4}$$

where σ_α denotes the standard deviation of the disorder and L_c denotes the correlation length of the disorder in units of the number of rings. For this disorder model, rather than trying to fit individual spectra, we analyzed the statistical properties of the simulated spectra of individual disordered aggregates, such as the correlation plots for the two linewidths (see Fig. 1) and histograms for the linewidths and peak positions, and compared those to the experiment. We discovered that in order to get good comparison with the experiment, a model including only disorder in α does not suffice (see Sec. IV C), and we also have to include disorder in the second angle that describes the molecular orientations, β. In this extended model, we use a similar correlated distribution as Eq. (3) for the angles β_n, with mean $\langle\beta\rangle$ and standard deviation σ_β. The correlation length for this distribution is assumed to be the same L_c as for the α distribution.

B. Results for segment model

Using the segment disorder model described above, the measured polarization dependent spectra of four individual tubes were fitted. Out of the 52 spectra of single tubes available from the study reported in Ref. 45, we selected the four that were also studied in more detail in that publication because they span much of the variation of the 52 experimental spectra. We refer to these aggregates as aggregate 1 up to aggregate 4, in the same way as was done in Ref. 45. All four aggregates exhibit the linewidth anomaly, as is evident from their positions in the linewidth correlation plot of Fig. 1, indicated by the crosses. The measured polarization dependent spectra for these aggregates are shown in Fig. 4, left column.

The fit procedure was as follows. We first generated a library of theoretical absorption spectra for light polarized parallel and perpendicular to the tube's axis, $I^{\parallel}_{\text{theory}}(\alpha_i, E)$ and $I^{\perp}_{\text{theory}}(\alpha_i, E)$, respectively, for homogeneous tubes with $\alpha = \alpha_i$ varying in steps of 0.1° between 30° and 50°, a range that widely covers all α values required in Ref. 45 to fit the spectra without disorder. Here, as mentioned above, E denotes the photon energy of the exciting field. When creating this library, we used a constant length of $N_1 = 1000$ for the homogeneous tube. This value does not indicate the length of individual segments; it is used to ensure that the spectra in the library have reached the long-tube limit, where we assume that individual segments are long enough for this limit to apply. For a single aggregate with a particular realization of segment disorder, the theoretical spectrum in both polarization directions is obtained by averaging the respective spectra for different α_i values weighted by their occurrence c_i^2 in that realization, which is characterized by the histogram for the α disorder realization defined in Sec. IV A (i.e., c_i^2 is the height of the histogram in the ith bin). We note that in the segment model, the total tube length is not fixed; only the relative weights c_i^2 are.

The optimal set of weights c_i^2 for a particular aggregate studied in the experiment was determined by requiring the best simultaneous fits to its experimental spectrum $I^{\parallel}_{\text{experiment}}(E)$ for the polarization angle at which the lower-energy peak (with parallel polarization) reaches its maximum and to the experimental spectrum $I^{\perp}_{\text{experiment}}(E)$ for a polarization angle that is shifted over 90° relative to the first angle. In the experimental spectra in Fig. 4, these two polarization angles are indicated by the cyan and orange lines, respectively. This simultaneous optimization is reached by minimizing the error, defined as

$$\varepsilon = \sum_{i,j,s} \left(c_i^2 I^s_{\text{theory}}(\alpha_i, E_j) - I^s_{\text{experiment}}(E_j) \right)^2, \tag{5}$$

where j labels the discretized set of energies and s labels the two polarization directions. The minimization of the error was performed using the "fminsearch" command of MATLAB, which is a multidimensional unconstrained nonlinear minimization derivative-free method.[72] We note that in these calculations, the angles β and γ for each one of the four aggregates considered were taken identical to those that generated the best fits in Ref. 45; see Table I.

The results for the fits for the four selected aggregates are displayed in the center column of Fig. 4, for both polarization directions. The right column of Fig. 4 displays the histogram of the α values that characterizes the disorder realization underlying the best fit, and Table I presents the mean $\langle\alpha\rangle$ and standard deviation σ_α characterizing this histogram for each one of the four aggregates.

Clearly, the segment model yields excellent fits for all four aggregates considered. Since these four aggregates were selected to span the variation of most of the 52 experimental spectra observed in Ref. 45, we are confident that any of those experimental spectra can be fitted using this model. The histograms show that the α distribution that fits each one of the spectra best has a standard deviation of a few degrees and a mean value that is very close to the α value that gave the best model fits without intra-aggregate disorder (last column in Table I).[45] The advantage of the current approach over the one in Ref. 45 is that it offers an explanation of the linewidth anomaly in terms of a narrow disorder distribution in the molecular orientations, as is evident from the quality of the fits of both absorption lines. The fact that such small amounts of disorder in α may explain the anomaly is rooted in the much stronger α dependence of the lower-exciton energy than the higher-energy one, as depicted in Fig. 3(a).

C. Results for continuous disorder model

Above, we found excellent fits to the single-tube spectra using a segment model of disorder in the angle α. It should be realized that the quality of the fits is made possible not only by the fact that disorder in α gives a larger linewidth to the lower-energy band but also because a large set of parameters (the weights c_i^2) may be varied to obtain the fits. We also note that these fits require many segments to be present in a single tube, implying that they may only be obtained for tubes containing many thousands of rings, which may go beyond the typical aggregate length in the experiment or the area of the (diffraction-limited) focus of the excitation light. Of course, a strictly segmented realization of the disorder, while appealing in its simplicity and facilitating finding disorder realizations that fit individual spectra, is only one limit of the more general way of introducing correlated continuous disorder in the aggregates.[70] For these reasons, in this section, we explore the more advanced model

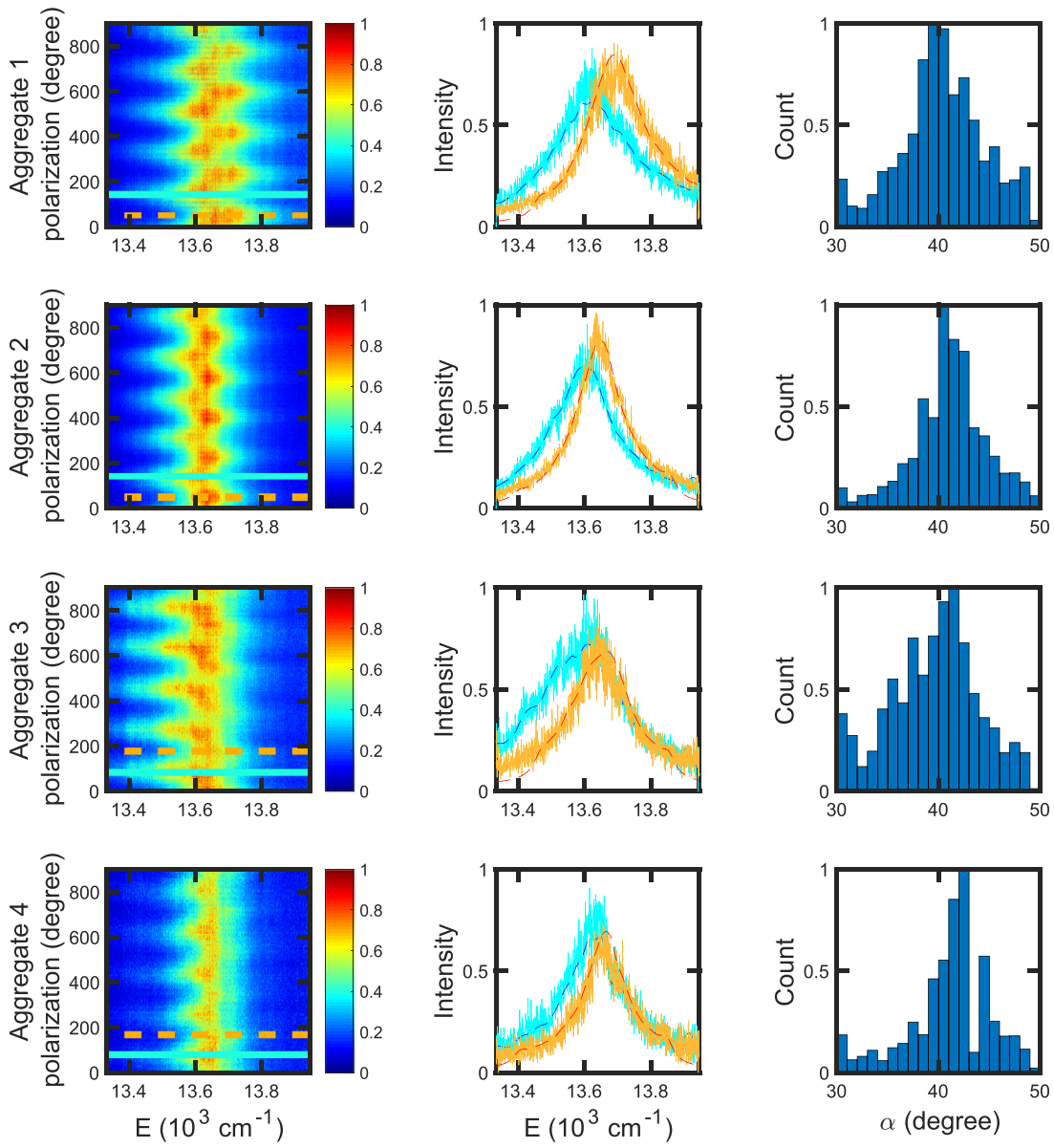

FIG. 4. Left column: Fluorescence excitation spectra of four different ZnChl aggregates as a function of polarization angle of the exciting light on the substrate on which the tubular aggregates lie (tubes' axes in the plane of the substrate) reported in Ref. 45; the cyan solid line indicates the polarization angle at which the low-energy spectral peak reaches its maximum height; the orange dashed line is shifted over 90° relative to the cyan one. Middle column: Spectra obtained at the cross sections indicated by the cyan and orange lines in the left column, together with the best fits (dashed thin lines) obtained for these two polarization angles using the segment model of disorder in the angle α. Right column: The histograms for the distribution of α that give the spectral fits in the middle column, binned per degree. The parameters used in the calculations are given at the start of Sec. IV; the length of the tubes is not fixed in the segment model (see text).

with continuous disorder in the molecular orientations, presented in Sec. IV A.

Using the continuous disorder model, we calculated absorption spectra for a large number of individual tubular aggregates, each spectrum separated in polarization directions parallel and perpendicular to the tube's axis, respectively. In these calculations, the parameters N_2, R, h, $\hbar\omega_0$, and Γ_q were taken as above, as was the magnitude of the molecular transition dipoles (see start of Sec. IV). The length of each tube was set to $N_1 = 1000$ rings, which corresponds to 670 nm and falls in the experimental length range of 100 nm to several micrometers.[46] For each aggregate, we generated a realization of the disorder in α by drawing correlated random

TABLE I. Mean values of α and the standard deviation σ_α in this angle obtained from the histograms in the right column of Fig. 4, together with the values of β and γ used to fit the spectra of aggregates 1–4. In the last column, the fixed value of α is shown that was used to analyze the data for each one of the four aggregates in Ref. 45 without intra-aggregate disorder.

Aggregate	$\langle\alpha\rangle$ (deg)	σ_α (deg)	β (deg)	γ (deg)	α (deg) (Ref. 45)
1	40.6	4.5	54.2	10.0	39.9
2	41.3	3.9	52.4	9.0	41.5
3	39.9	4.8	48.4	14.0	40.5
4	41.6	4.4	51.2	10.5	42.4

values from the distribution equation (3) and similarly for the angles β. For the aggregate length considered and the disorder strengths σ_α and σ_β that turn out to be relevant, the spectra of individual tubes in both polarization directions show a main peak with minor substructure. We characterized the simulated spectra by the positions E_- and E_+ of the lower- and higher-energy main peaks, respectively (polarized along and perpendicular to the tube's axis), as well as the separation ΔE between both peaks. Moreover, we also obtained the linewidths (FWHM) of both peaks as W_- and W_+.

Rather than trying to find the realizations of continuous disorder that happen to generate theoretical spectra that match observed spectra of single nanotubes (which, as opposed to the segment model, would be a practically impossible job in the current model), we compared the statistical properties of the simulated spectra to the statistics found in the experiment. In particular, we used the mean values $\langle\alpha\rangle$ and $\langle\beta\rangle$, the standard deviations σ_α and σ_β, the correlation length L_c, and the value of the fixed helical angle γ as free parameters to obtain a good match between theory and experiment for the linewidth correlation plot of Fig. 1 and for the distributions of W_-, W_+, E_-, E_+, and ΔE (the latter five distributions were all reported in Ref. 45). Given the limited experimental statistics, determined by the number (52) of tubes for which the spectra were measured, we have not aimed at minimizing a rigorously defined error in the global comparison between the theoretical and experimental statistical properties but instead have judged by eye and from their mean values and standard deviations to what extent the various distributions match.

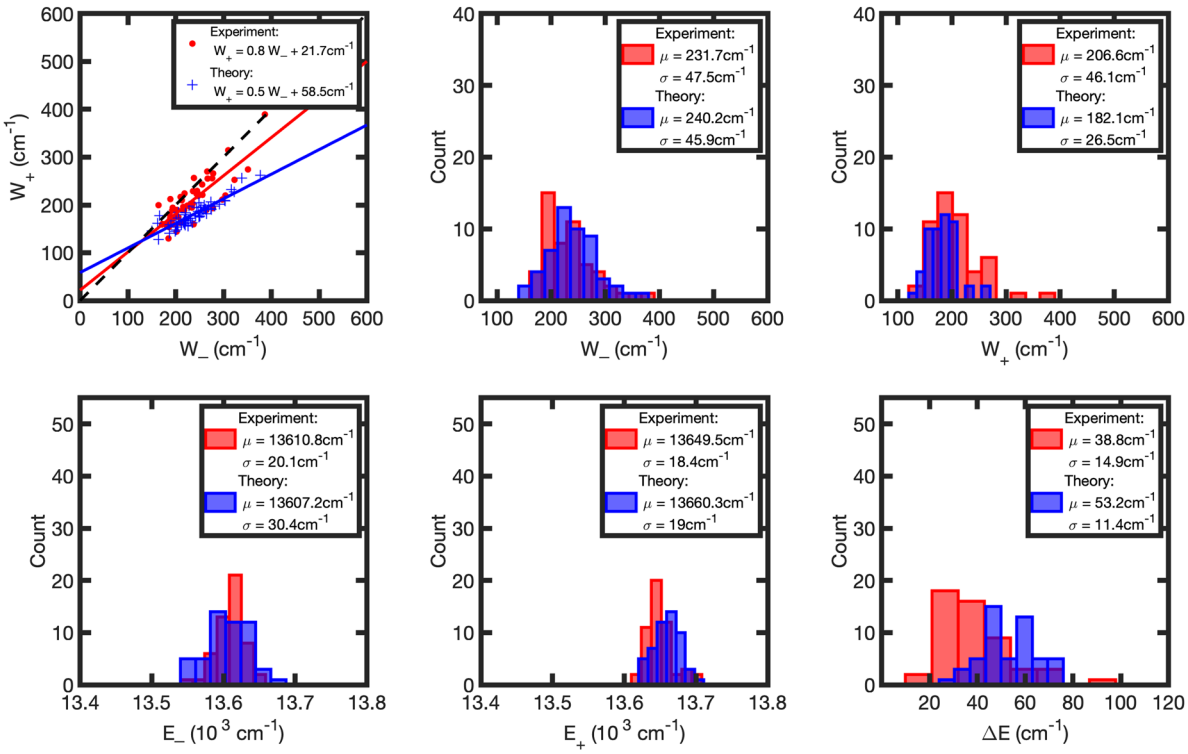

FIG. 5. Comparison between theory (blue) and experiment (red) for the linewidth correlation plot and the distributions for W_-, W_+, E_-, E_+, and ΔE including continuous disorder in α only. The experimental data for the latter five distributions are taken from Ref. 45. The panel for the correlation plot also gives the best linear regressions through the experimental and theoretical data points, with the corresponding slopes and offsets; the other panels give the mean values and standard deviations for the experimental and theoretical distributions. For the calculations, we used $\langle\alpha\rangle = 41.1°$, $\sigma_\alpha = 2.5°$, and $L_c = 70$ rings. The angles β and γ were set to fixed values of 51.6° and 10.9°, respectively, being the averages of the values for these angles used to fit the spectra for aggregates 1–4 in Ref. 45. All other parameters were chosen as indicated at the start of Sec. IV, except for the homogeneous linewidths, for which we used $\Gamma_- = 80\ \text{cm}^{-1}$ for transitions with polarization parallel to the tube's axis and $\Gamma_+ = 100\ \text{cm}^{-1}$ for the perpendicular transitions. The length of the simulated aggregates was set to $N_1 = 1000$ rings (see text).

From our calculations, we found that the phenomenon of the anomalous linewidth correlation can be qualitatively explained using only continuous disorder in α (i.e., setting the angle β to a fixed value), but the linear regression of the theoretical data points always has a significantly smaller slope than the one for the experimental points in Fig. 1, even if we try to tune this plot by using different homogeneous linewidths Γ_q for the lower- and higher-energy exciton transitions. The closest to a good agreement between the theoretical and experimental statistics is shown in Fig. 5 and was obtained for parameters quoted in the caption, where we had to adjust Γ_q as indicated in the caption in order to reach this level of agreement. We observe that most of the histograms in Fig. 5 give a reasonable to very good match between theory and experiment, with most discrepancy observed for the W_+ and the ΔE distributions. We clearly see, however, that within this model, the linewidth correlation has much too small a slope, which, in fact, implies that the effect of disorder in α is overestimated; thus, σ_α should be reduced, but then, another source of disorder has to be introduced in order to match the standard deviations of the distributions for the individual linewidths W_- and W_+ to the experiment.

To repair the above deficiencies of the model, we have introduced disorder in β as well, which is physically plausible to occur, as it is the other angle characterizing the molecular dipole orientations. Figure 3 demonstrates that this will not affect the linewidth anomaly, as both the upper and lower exciton energies depend about equally strong on β. It will add additional width contributions to both spectral peaks, however, which is what we need if we lower σ_α. Figure 6 gives the comparison between theory and experiment for the system parameters that result in the best agreement. To achieve this, we had to lower σ_α to 1.0°, while the disorder in β was taken to be $\sigma_\beta = 2.0°$, both with a correlation length of $L_c = 40$ rings. The helical angle was taken $\gamma = 7.1°$ in order to match the average of the theoretical distributions of both peak positions to those obtained from the experiment; the precise choice of γ within margins of up to the order of 10° hardly affects the width of the distributions of the positions and the statistics of the spectral widths.

We observe that with the exception of the distribution of ΔE, all panels in Fig. 6 show a good agreement between theory and experiment. In particular, we note that the linewidth anomaly is now not only recovered qualitatively but also quantitatively: the linear regression of the theoretical data points shows a good agreement with that of the experimental data. The theoretical and experimental distributions of the peak positions and linewidths are also in good agreement, as is also clear from their mean values and standard

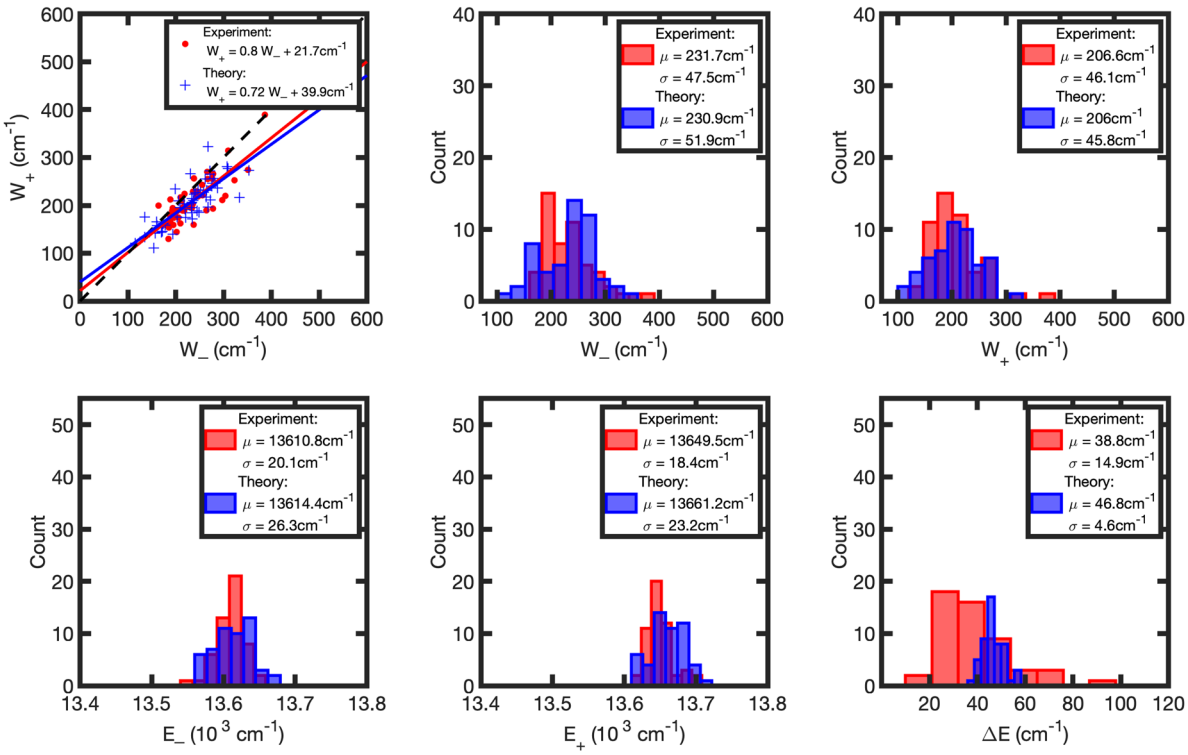

FIG. 6. Comparison between theory (blue) and experiment (red) for the linewidth correlation plot and the distributions for W_-, W_+, E_-, E_+, and ΔE, allowing for continuous disorder in α and β. The experimental data for the latter five distributions are taken from Ref. 45. The panel for the correlation plot also gives the best linear regressions through the experimental and theoretical data points, with the corresponding slopes and offsets; the other panels give the mean values and standard deviations for the experimental and theoretical distributions. For the calculations, we used $\langle\alpha\rangle = 42.2°$, $\sigma_\alpha = 1.0°$, $\langle\beta\rangle = 52.7°$, $\sigma_\beta = 2.0°$, and $L_c = 40$ rings. The angle γ was set to the fixed value of 7.1°. All other parameters were chosen as indicated at the start of Sec. IV; the homogeneous width of all exciton transitions was taken to be $\Gamma_q = 50\ \text{cm}^{-1}$. The length of the simulated aggregates was set to $N_1 = 1000$ rings (see text).

deviations given in the insets. However, the distribution for the energy difference ΔE between both spectra peaks is not correctly recovered in this model; in particular, its width is strongly underestimated. As the separate distributions for both peak positions, E_- and E_+, are fitted very well, this implies that in the current model, the correlation between both peak positions is overestimated. Stronger disorder in the angle α would partially undo this correlation, as is clear from the ΔE distribution in Fig. 5, but that generates other disagreements, as we have seen.

It is conceivable that besides the intra-aggregate disorder modeled here, there is also an inter-aggregate disorder component, for instance, the mean value $\langle\alpha\rangle$ may vary between aggregates. This would not change the linewidths for the individual tubes and, hence, not change their distributions and correlation plot, but it would affect the positions (mainly E_-) and, in particular, would broaden the ΔE distribution. Combining the information from Figs. 5 and 6, it appears that such additional inter-aggregate disorder in α would have to have a standard deviation in the order of 1.0°–1.5° to recover the experimental ΔE distribution; however, its inclusion would require fine tuning other parameters again. We have not attempted to carry this idea further by doing actual simulations including inter-aggregate disorder, as it would require finding the optimum in an even wider range of free parameters; if one allows for inter-aggregate disorder in α, there is no reason not to allow for it in β.

We have tested the sensitivity of fitting the experimentally observed statistical properties to the model parameters characterizing the disorder (namely, the mean values $\langle\alpha\rangle$ and $\langle\beta\rangle$, the standard deviations σ_α and σ_β, and the correlation length L_c), by repeating simulations for a variety of combinations of values for these parameters. To give an impression of this sensitivity, we present in the appendix an overview of changes in the statistical properties when changing, in particular, σ_α, σ_β, and L_c around their optimal values that led to the fits displayed in Fig. 6. We note that for several separate quantities, better agreement to experiment is, in fact, possible by changing one of the disorder parameters, but that such a change inevitably deteriorates the quality of the fit of one of the other quantities even more.

To end this section, we note that in the experiment, an effective distribution for the angle β was also obtained through the ratio of the oscillator strengths in both peaks (see end of Sec. III A).[45] The standard deviation of that distribution was found to be 4.3°, which is about twice as big as the one we used to get the fits in Fig. 6. This discrepancy could be another effect of inter-aggregate disorder (in β) but could also result from the fact that the tubes in the experiment may be bent,[46] which affects the ratio of oscillator strengths in both peaks.

V. CONCLUSION

In this paper, we have studied the occurrence of disorder within nanotubular self-assembled ZnChl aggregates. As experimental markers for disorder, we have used the statistical properties of the two optical bands that characterize these aggregates as obtained from polarization resolved fluorescence excitation experiments on single nanotubes. These experiments reveal that the lower-energy exciton band of single nanotubes typically has a larger width than the upper exciton band, which indicates that this width is not determined by homogeneous (lifetime) broadening only and must be caused at least, in part, by inhomogeneous broadening (disorder) within each aggregate. By modeling the spectra using numerical simulations, we have shown that small disorder (a few degrees) in the orientations of individual molecules within the aggregate may explain the observed correlation between both linewidths quantitatively.

To interpret the experiments, we have used two models of orientational disorder. In the first model, the orientations were assumed constant within finite but long segments of the aggregate. By adjusting the occurrence of segments with particular orientations, we were able to generate excellent fits of the experimental polarization resolved spectra of individual nanotubes. The quality of the fits is, *inter alia*, made possible by the very large amount of freedom to vary parameters in this model. In a more advanced model, we allowed for continuous variation of the molecular orientations within the aggregate, with a certain standard deviation and correlation length. We demonstrated that small orientational disorder (order 2°) correlated over several tens of nm may not only explain the linewidth correlation but also explain other statistical properties of the spectra obtained from the experiment, such as the distributions of peak positions and linewidths. Within the model used, the width of the distribution of energy separations between both peaks is significantly underestimated; we have argued that this may result from inter-aggregate disorder, which was not taken into account.

The importance of this work lies in the realization that single-aggregate experiments in combination with systematic exciton modeling may be used to disentangle sources of disorder in and between different aggregates, whose markers would get lost in ensemble spectroscopies,[73,74] which cannot be resolved by high-resolution imaging techniques such as AFM or electron microscopy. The conclusion that the aggregates studied suffer from disorder in the molecular orientations of the order of a few degrees is physically plausible. Indeed, molecular dynamics simulations of other dye aggregates have revealed that such disorder may easily occur.[32,34] It is interesting that polarization resolved single-aggregate experiments are sensitive to such small variations, which shows the power of this technique in unraveling the molecular basis for the functional properties of large aggregates.

We express caution, though, that our model results should not be overinterpreted as they still are limited by the sources of disorder considered. For instance, we have not included energy disorder in our model because, as we argued, the linewidth correlation strongly suggests that orientational disorder must be a dominant factor to explain it; at the same time, energy disorder caused by random solvent shifts generally plays a role in molecular aggregates. In addition, as mentioned, we did not include inter-aggregate disorder, for instance, by allowing the mean values of the orientational distributions to differ between aggregates. Of course, including all possible sources of intra- and inter-aggregate disorder would generate more freedom to improve the fits but would be a formidable job to explore systematically, and its value would be restricted by the fact that the experimentally available data obtained from several tens of aggregates, then, may become a limiting factor to draw solid conclusions. This points out the importance of future experimental and theoretical steps to further improve the perspective of a full molecular-scale understanding of the properties of molecular

TABLE II. Presentation of the statistical properties of spectra simulated using the continuous disorder model when varying the three model parameters σ_α, σ_β, and L_c around their optimal values that generated the fits in Fig. 6. The first column names the statistical property considered (where μ indicates its mean and σ its standard deviation; Slope_W is the slope of the linear regression of the linewidth correlation plot, and W_+ intercept its intercept), the second column presents the experimental value, the third column shows the value obtained in the optimal fit of Fig. 6 (where $\sigma_\alpha = 1°$, $\sigma_\beta = 2°$, and $L_c = 40$ rings), and the remaining columns display the variations when changing the model parameters characterizing the disorder as indicated above each column. In all cases displayed, only one parameter was changed at a time (for instance, in the column where σ_α is varied, the results are quoted keeping σ_β and L_c at their optimal values). The full search for the optimal fit was not restricted to only changing one model parameter at a time.

Statistical properties	Experiment	Best fit	σ_α (deg)		σ_β (deg)		L_c (rings)	
			0.5	1.5	1.5	2.5	20	60
Slope_W	0.8	0.72	0.87	0.62	0.75	0.59	0.63	0.72
W_+intercept (cm^{-1})	21.7	39.9	12.3	61.2	22.6	82.1	50.4	38.8
μ_{W_-} (cm^{-1})	231.7	230.9	197.2	264.6	201	259.4	225.8	237.6
σ_{W_-} (cm^{-1})	47.5	51.9	38.3	61.9	40.8	61.2	42.1	60.3
μ_{W_+} (cm^{-1})	206.6	206	183.3	226.2	172.7	236.2	192.5	209
σ_{W_+} (cm^{-1})	46.1	45.8	39.1	51.8	35.8	55.5	36.7	52.9
μ_{E_-} (cm^{-1})	13 610.8	13 614.4	13 616.2	13 612.7	13 618.3	13 610	13 616.1	13 613.4
σ_{E_-} (cm^{-1})	20.1	26.3	21.6	31	22.1	30.4	18.8	32
μ_{E_+} (cm^{-1})	13 649.5	13 661.2	13 660.7	13 661.7	13 660.3	13 662.5	13 662.7	13 660.1
σ_{E_+} (cm^{-1})	18.4	23.2	20.2	26.1	18.9	27.4	16.6	28.3
$\mu_{\Delta E}$ (cm^{-1})	38.8	46.8	44.6	49	42.1	52.5	46.6	46.6
$\sigma_{\Delta E}$ (cm^{-1})	14.9	4.6	3.2	6.2	3.8	5.7	3.2	5.5

aggregates. On the theoretical side, also a first-principle type of analysis of molecular packing and disorder could add important input for the phenomenological approach used here.[34,63]

ACKNOWLEDGMENTS

The experimental data used for benchmarking in this paper have been taken on ZnChl aggregates prepared by Frank Würthner (University of Würzburg, Germany) and co-workers and have been published before, as cited. Financial support from the German Science Foundation (DFG, J. Köhler: Grant Nos. KO-1359/26-1 and GRK 1640), the State of Bavaria in the framework of the Collaborative Research Network "Solar Technologies go Hybrid" (A.L. and J. Köhler), the Elite Network of Bavaria (ENB) program "Macromolecular Science" (J. Köhler), and the Bavarian Polymer Institute (BPI, KeyLabs for Electron and Optical Microscopy and for Supramolecular Polymers; A.L. and J. Köhler) is gratefully acknowledged.

APPENDIX: SENSITIVITY OF STATISTICAL PROPERTIES TO THE MODEL PARAMETERS

Table II shows the sensitivity of the statistical properties of the simulated spectra for the model whose results are presented in Fig. 6, to the parameters that characterize the intra-aggregate disorder, namely σ_α, σ_β, and L_c.

DATA AVAILABILITY

The data that support the findings of this study are available from the corresponding author upon reasonable request.

REFERENCES

[1] E. E. Jelley, Nature **138**, 1009 (1936).
[2] G. Scheibe, Angew. Chem. **50**, 212 (1937).
[3] E. W. Knapp, Chem. Phys. **85**, 73 (1984).
[4] F. C. Spano and S. Mukamel, J. Chem. Phys. **91**, 683 (1989).
[5] S. De Boer and D. A. Wiersma, Chem. Phys. Lett. **165**, 45 (1990).
[6] F. C. Spano and S. Mukamel, Phys. Rev. A **40**, 5783 (1989).
[7] J. Knoester, Chem. Phys. Lett. **203**, 371 (1993).
[8] J. Knoester and F. C. Spano, Phys. Rev. Lett. **74**, 2780 (1995).
[9] I. G. Scheblykin, O. Y. Sliusarenko, L. S. Lepnev, A. G. Vitukhnovsky, and M. Van der Auweraer, J. Phys. Chem. B **105**, 4636 (2001).
[10] A. T. Haedler, K. Kreger, A. Issac, B. Wittmann, M. Kivala, N. Hammer, J. Köhler, H.-W. Schmidt, and R. Hildner, Nature **523**, 196 (2015).
[11] A. R. Holzwarth, K. Griebenow, and K. Schaffner, J. Photochem. Photobiol., A **65**, 61 (1992).
[12] A. M. van Oijen, M. Ketelaars, J. Köhler, T. J. Aartsma, and J. Schmidt, Science **285**, 400 (1999).
[13] H. van Amerongen, L. Valkunas, and R. van Grondelle, *Photosynthetic Excitons* (World Scientific, 2000).
[14] R. E. Blankenship, *Molecular Mechanisms of Photosynthesis* (Blackwell Science, 2002).
[15] G. R. Fleming and G. D. Scholes, Nature **431**, 256 (2004).
[16] R. J. Cogdell, A. Gall, and J. Köhler, Q. Rev. Biophys. **39**, 227 (2006).
[17] G. T. Oostergetel, H. van Amerongen, and E. J. Boekema, Photosynth. Res. **104**, 245 (2010).
[18] G. D. Scholes, G. R. Fleming, A. Olaya-Castro, and R. van Grondelle, Nat. Chem. **3**, 763 (2011).
[19] T. Mirkovic, E. E. Ostroumov, J. M. Anna, R. van Grondelle, Govindjee, and G. D. Scholes, Chem. Rev. **117**, 249 (2017).
[20] M. Kasha, Radiat. Res. **20**, 55 (1963).
[21] N. J. Hestand, R. Tempelaar, J. Knoester, T. L. C. Jansen, and F. C. Spano, Phys. Rev. B **91**, 195315 (2015).
[22] N. J. Hestand and F. C. Spano, Acc. Chem. Res. **50**, 341 (2017).

[23]T. Brixner, R. Hildner, J. Köhler, C. Lambert, and F. Würthner, Adv. Energy Mater. **7**, 1700236 (2017).
[24]M. Schreiber and Y. Toyozawa, J. Phys. Soc. Jpn. **51**, 1528 (1982).
[25]H. Fidder, J. Knoester, and D. A. Wiersma, J. Chem. Phys. **95**, 7880 (1991).
[26]V. A. Malyshev, Opt. Spectrosc. **71**, 505 (1991).
[27]S. Jang, S. E. Dempster, and R. J. Silbey, J. Phys. Chem. B **105**, 6655 (2001).
[28]C. Didraga, A. Pugžlys, P. R. Hania, H. von Berlepsch, K. Duppen, and J. Knoester, J. Phys. Chem. B **108**, 14976 (2004).
[29]F. C. Spano, J. Chem. Phys. **122**, 234701 (2005).
[30]J. Adolphs, F. Müh, M. E.-A. Madjet, and T. Renger, Photosynth. Res. **95**, 197 (2008).
[31]J. Huh, S. K. Saikin, J. C. Brookes, S. Valleau, T. Fujita, and A. Aspuru-Guzik, J. Am. Chem. Soc. **136**, 2048 (2014).
[32]F. Haverkort, A. Stradomska, A. H. de Vries, and J. Knoester, J. Phys. Chem. A **118**, 1012 (2014).
[33]C. P. van der Vegte, J. D. Prajapati, U. Kleinekathöfer, J. Knoester, and T. L. C. Jansen, J. Phys. Chem. B **119**, 1302 (2015).
[34]A. S. Bondarenko, I. Patmanidis, R. Alessandri, P. C. T. Souza, T. L. C. Jansen, A. H. de Vries, S.-J. Marrink, and J. Knoester, "Multiscale modeling of molecular structure and optical properties of complex supramolecular aggregates," Chem. Sci. (to be published).
[35]A. Boukahil and D. L. Huber, J. Lumin. **48-49**, 255 (1991).
[36]A. Merdasa, Á. J. Jiménez, R. Camacho, M. Meyer, F. Würthner, and I. G. Scheblykin, Nano Lett. **14**, 6774 (2014).
[37]E. A. Bloemsma, S. M. Vlaming, V. A. Malyshev, and J. Knoester, Phys. Rev. Lett. **114**, 156804 (2015).
[38]A. S. Bondarenko, T. L. C. Jansen, and J. Knoester, J. Chem. Phys. **152**, 194302 (2020).
[39]L. Cleary and J. Cao, New J. Phys. **15**, 125030 (2013).
[40]C. Chuang, C. K. Lee, J. M. Moix, J. Knoester, and J. Cao, Phys. Rev. Lett. **116**, 196803 (2016).
[41]V. A. Malyshev and F. Domínguez-Adame, Chem. Phys. Lett. **313**, 255 (1999).
[42]A. M. van Oijen, M. Ketelaars, J. Köhler, T. J. Aartsma, and J. Schmidt, Biophys. J. **78**, 1570 (2000).
[43]L. M. Günther, M. Jendrny, E. A. Bloemsma, M. Tank, G. T. Oostergetel, D. A. Bryant, J. Knoester, and J. Köhler, J. Phys. Chem. B **120**, 5367 (2016).
[44]E. Lang, A. Sorokin, M. Drechsler, Y. V. Malyukin, and J. Köhler, Nano Lett. **5**, 2635 (2005).
[45]A. Löhner, T. Kunsel, M. I. S. Röhr, T. L. C. Jansen, S. Sengupta, F. Würthner, J. Knoester, and J. Köhler, J. Phys. Chem. Lett. **10**, 2715 (2019).
[46]S. Sengupta, D. Ebeling, S. Patwardhan, X. Zhang, H. von Berlepsch, C. Böttcher, V. Stepanenko, S. Uemura, C. Hentschel, H. Fuchs, F. C. Grozema, L. D. A. Siebbeles, A. R. Holzwarth, L. Chi, and F. Würthner, Angew. Chem., Int. Ed. **51**, 6378 (2012).
[47]C. Spitz, J. Knoester, A. Ouart, and S. Daehne, Chem. Phys. **275**, 271 (2002).
[48]T. S. Balaban, H. Tamiaki, and A. R. Holzwarth, "Chlorins programmed for self-assembly," in *Supermolecular Dye Chemistry* (Springer, Berlin, Heidelberg, 2005), pp. 1–38.
[49]D. M. Eisele, C. W. Cone, E. A. Bloemsma, S. M. Vlaming, C. G. F. van der Kwaak, R. J. Silbey, M. G. Bawendi, J. Knoester, J. P. Rabe, and D. A. Vanden Bout, Nat. Chem. **4**, 655 (2012).
[50]D. Abramavicius, A. Nemeth, F. Milota, J. Sperling, S. Mukamel, and H. F. Kauffmann, Phys. Rev. Lett. **108**, 067401 (2012).
[51]K. A. Clark, C. W. Cone, and D. A. Vanden Bout, J. Phys. Chem. C **117**, 26473 (2013).
[52]J. R. Caram, S. Doria, D. M. Eisele, F. S. Freyria, T. S. Sinclair, P. Rebentrost, S. Lloyd, and M. G. Bawendi, Nano Lett. **16**, 6808 (2016).
[53]S. Shoji, T. Ogawa, T. Hashishin, S. Ogasawara, H. Watanabe, H. Usami, and H. Tamiaki, Nano Lett. **16**, 3650 (2016).
[54]C. Friedl, T. Renger, H. V. Berlepsch, K. Ludwig, M. Schmidt am Busch, and J. Megow, J. Phys. Chem. C **120**, 19416 (2016).
[55]B. Kriete, A. S. Bondarenko, V. R. Jumde, L. E. Franken, A. J. Minnaard, T. L. C. Jansen, J. Knoester, and M. S. Pshenichnikov, J. Phys. Chem. Lett. **8**, 2895 (2017).
[56]Y. Wan, A. Stradomska, J. Knoester, and L. Huang, J. Am. Chem. Soc. **139**, 7287 (2017).
[57]S. Doria, T. S. Sinclair, N. D. Klein, D. I. G. Bennett, C. Chuang, F. S. Freyria, C. P. Steiner, P. Foggi, K. A. Nelson, J. Cao, A. Aspuru-Guzik, S. Lloyd, J. R. Caram, and M. G. Bawendi, ACS Nano **12**, 4556 (2018).
[58]M. Gullì, A. Valzelli, F. Mattiotti, M. Angeli, F. Borgonovi, and G. L. Celardo, New J. Phys. **21**, 013019 (2019).
[59]G. L. Celardo, M. Angeli, T. J. A. Craddock, and P. Kurian, New J. Phys. **21**, 023005 (2019).
[60]V. I. Prokhorenko, D. B. Steensgaard, and A. R. Holzwarth, Biophys. J. **85**, 3173 (2003).
[61]X. Li, F. Buda, H. J. M. de Groot, and G. J. A. Sevink, J. Phys. Chem. C **122**, 14877 (2018).
[62]L. M. Günther, A. Löhner, C. Reiher, T. Kunsel, T. L. C. Jansen, M. Tank, D. A. Bryant, J. Knoester, and J. Köhler, J. Phys. Chem. B **122**, 6712 (2018).
[63]X. Li, F. Buda, H. J. M. de Groot, and G. J. A. Sevink, J. Phys. Chem. C **123**, 16462 (2019).
[64]X. Li, F. Buda, H. J. M. de Groot, and G. J. A. Sevink, J. Phys. Chem. B **124**, 4026 (2020).
[65]C. Didraga, J. A. Klugkist, and J. Knoester, J. Phys. Chem. B **106**, 11474 (2002).
[66]C. Didraga and J. Knoester, Chem. Phys. **275**, 307 (2002).
[67]M. V. Mostovoy and J. Knoester, J. Phys. Chem. B **104**, 12355 (2000).
[68]C. Hofmann, T. J. Aartsma, and J. Köhler, Chem. Phys. Lett. **395**, 373 (2004).
[69]A. Tilgner, H. P. Trommsdorff, J. M. Zeigler, and R. M. Hochstrasser, J. Chem. Phys. **96**, 781 (1992).
[70]J. Knoester, J. Chem. Phys. **99**, 8466 (1993).
[71]F. C. Spano, J. Chem. Phys. **116**, 5877 (2002).
[72]MATLAB, version 2015b, The MathWorks, Inc., Natick, Massachusetts, 2015.
[73]S. Jang and R. J. Silbey, J. Chem. Phys. **118**, 9324 (2003).
[74]R. J. Cogdell and J. Köhler, Biochem. J. **422**, 193 (2009).